APPENDIX A: Data and analytical techniques

Zircon concentrates were obtained by standard separation techniques: crushing, sieving, heavy liquids, and magnetic separation. Selected zircon crystals were hand-picked from concentrates using high power (160x) stereo-zoom microscropes with cross-polarization for inclusion screening; however, most of the investigated zircons did contain small (~5-20 σm) visible inclusions.

U/Pb dating

A Lambda Physik LPX 120I ArF excimer laser with a 193 nm wavelength and 29 micron beam diameter operating at 5 Hz was used to ablate holes in unpolished zircons from the Navajo Sandstone, standard zircons, and NIST 610 glass exposed on sticky tape in a sample cell connected to an Agilent 7500S ICP-MS. The method is generally that reported in Eggins and Shelley (2002). The cell was under a positive gas pressure of Ar and He with their gas port geometries arranged so that a stratified flow of He carried the sample away from the ablation site and the mixed gas carried the ablated sample through a smoothing manifold and into the ICP-MS. Note that analysis of unknowns on a rough surface produces a noisier signal than those analyzed on a flat one. Masses of isotopes used in geochronology (^{206}Pb, ^{207}Pb, ^{208}Pb, ^{232}Th, ^{235}U, and ^{238}U) were each analysed for 0.04 s, and other elements of geochemical interest (^{29}Si, ^{31}P, ^{91}Zr, ^{177}Hf, and 7 REE^{s}) were each collected for 0.01 s. Data were collected in peak jumping mode with a mass sweep time of 0.384 seconds. As an indicator of sensitivity, background-corrected ^{208}Pb produced ~1650 cps/ppm on NIST 610. Background levels (in "laser off" mode) were collected for about 20 s at the beginning of each analysis, then a "laser on" signal was collected for 20 s with a material drilling rate of about 1 σm/s. The analysis menu consisted of R33 (zircon standard), NIST610, and then 5 unknowns resulting in 9 analyses on each of the standards and 40 analyses of unknowns. Two standards are necessary because 1) precision for geochronology requires down-hole fractionation effects on isotope ratios to be modelled from zircon and 2) an homogenous glass is required for calculating concentrations, especially Th/U, as standard zircons have uniform ages but are chemically inhomogenous. Background–corrected isotope ratios for concentration calculations were formed for each mass sweep for each analysis after a stable signal was achieved (about 5 s after laser-on), for Th/U and all other elements ratioed to ^{29}Si. Concentrations were derived using NIST610 as a standard, and assuming a stoichiometric concentration of SiO_2 of 37.22 wt% in the zircon. Zircon ^{232}Th/^{238}U is calculated assuming NIST 610 has ^{232}Th/^{238}U of 1.0187. Similarly, background–corrected isotope ratios for geochronology were formed for each mass sweep for each analysis after a stable signal was achieved (about 5 s after laser-on). U/Pb and Th/Pb ratios are then are normalized to the average standard zircon, R33, mass-sweep by mass-sweep. This standard is known to be concordant at 418.4+/-1 Ma (L.P. Black et al., in review). The measured uncertainties in the standard ratios used for chronology are incorporated into the quoted age uncertainties of the unknowns along with counting uncertainties in the analysis itself. The uncertainty on average R33 was 3.84% for ^{206}Pb/^{238}U and 2.57% for ^{207}Pb/^{206}Pb (1 ωstd dev). Most of this uncertainty derives from time-dependent ICP and laser drift but some probably derives from analysis on a rough surface. Common Pb content of zircons cannot be directly measured as counts on ^{204}Pb are low, and systemic Hg isobarically interferes. After these normalizations, common Pb is calculated and corrected for through the following steps. Using the initially calculated ^{206}Pb/^{238}U age direct from its ratio, the corresponding ^{208}Pb/^{232}Th on concordia is known and the ^{232}Th/^{238}U for the

zircon has been measured. The difference between the measured $^{208}Pb/^{232}Th$ and the one corresponding to the $^{206}Pb/^{238}U$ age (surplus or deficit) is attributed to common ^{208}Pb. Using the Cumming and Richards (1975) age-dependent Pb model, the number of atoms of ^{206}Pb and ^{207}Pb are calculated and subtracted from the corresponding U/Pb and $^{207}Pb/^{206}Pb$ ratios. This process is repeated until the $^{207}Pb/^{206}Pb$ ratio stops changing at a level corresponding to an age difference of 0.1 Ma. The resulting ratios allow the calculation of the "^{208}Pb-corrected $^{206}Pb/^{238}U$ and $^{207}Pb/^{206}Pb$ ages." The former is quoted for grains with ages less than 1300 Ma, and the latter for those older. Grains are deemed concordant if these two ages agree within 2% taking uncertainties into account. In this data set of 40 grains, 9 are discordant. ^{235}U is measured only for use when U signals are intense, and this circumstance was not encountered in this data set. Concordia plots for the zircons analyzed for this study are shown in Fig. DR1.

(U-Th)/He dating

Following U/Pb analysis, concordant zircons were retrieved and rinsed in acetone to avoid He-contamination from tape. (U-Th)/He ages were performed by Nd-YAG laser heating for He extraction, and sector ICP-MS for U-Th determinations, at Yale University. Crystals were measured and digitally photographed in at least 2 different orientations for ζ-ejection corrections. Crystals were placed in 1-mm Pt foil tubes, and loaded into stainless steel sample planchets with 32 sample slots. Planchets were loaded into a ~10 cm diameter laser cell with sapphire window, connected by high-vacuum flexhose to the He extraction/measurement line. Once in the laser cell and pumped down to a vacuum of $<10^{-7}$-10^{-8} torr, the crystal-bearing foil tubes were individually heated by lasing with about 1-5 W on the Nd-YAG for 20 minutes. Temperatures of heated foil packets were not measured, but from experiments relating luminosity and step-wise degassing of both apatite and zircon, we estimate typical heating temperatures of 1250-1400 °C for zircon. ^{4}He blanks (0.05-0.1 femtomol ^{4}He, after correction for spike ^{4}He) were determined by heating empty foil packets using the same procedure. Crystals were checked for quantitative degassing of He by sequential reheating. Gas liberated from samples was processed by: 1) spiking with ~0.4 pmol of ^{3}He, 2) cryogenic concentration at 16 K on a charcoal trap (condensation time calibrated for no significant $^{4}He/^{3}He$ fractionation), and purification by release at 37 K, followed by 3) measurement of $^{4}He/^{3}He$ ratios (corrected for HD and H_3 by monitoring H^+) on a quadrupole mass spectrometer next to a cold Zr-alloy getter. All ratios were referenced to multiple same-day measured ratios and known volumes of ^{4}He standards processed in the same way. Linearity of this standard referencing procedure has been confirmed over four orders of magnitude of ^{4}He intensity. ^{4}He standard reproducibility averages 0.2% on a daily and long-term (tank-depletion corrected) basis. Estimated 2ω analytical uncertainty on sample He determinations, including precision and accuracy from original manometric ^{4}He standard calibrations, is 1-2%.

Following degassing, samples were retrieved from the laser cell, spiked with a calibrated ^{229}Th and ^{233}U solution, dissolved in Teflon microvials in Parr bombs with HF and HNO_3, followed by either H_3BO_3 or another bomb run with HCl to remove fluoride salts, and a final dissolution in HNO_3. Each sample batch was prepared with a series of acid blanks and spiked normal solutions to check the purity and calibration of the reagents and spikes. Spiked solutions were analyzed as 0.5 ml of ~1-5 ppb U-Th solutions by isotope dilution on a Finnigan Element2 ICP-MS with a Teflon micro-flow nebulizer and double-pass spray chamber. Procedural U and Th blanks by this method are 1 ± 0.5 pg and 2 ± 1 pg, respectively. Routine in-run precisions and long-

term reproducibilities of standard $^{232}Th/^{229}Th$ and $^{238}U/^{233}U$ ratios are 0.1-0.4%, and estimated uncertainty on sample U-Th contents are estimated to be 1-2% (2ω).

To ensure that the laser ablation process does not mobilize helium, combined He-Pb ages were measured on single-crystals of the quickly-cooled Fish Canyon Tuff (Fig. DR2). He ages obtained from these zircons are similar to U/Pb ages for each sample, as well as to He ages from other Fish Canyon Tuff zircons that were analyzed by conventional (U-Th)/He methods. Replicate analyses of Durango apatite and Fish Canyon Tuff zircon during the period of these analyses yielded mean ages of 32.5 ± 1.5 Ma (2ω; ï = 42) and 28.3 ± 2.4 Ma (2ω; *n* = 37), respectively. On the basis of reproducibility of these and other intralab standards, we estimate an analytical uncertainty of 8% (2ω) for zircon in this study.

APPENDIX B: ζ-ejection correction for abraded detrital grains

For a description of the ζ-ejection problem for igneous and metamorphic zircons, see Farley et al. (1996). In brief, the ejection of alpha particles during the breakdown of U and Th will lead to a ~15 to 20 σm thick rim around the edge of the crystal that has an anomalously low concentration of He. During sedimentary transport of a detrital grain, this He-depleted rim, along with its ζ-ejection bias, can be removed due to grain abrasion. However, following deposition of the grain in the sedimentary environment, a new alpha ejection bias will develop.

We consider the case where the zircon He clock is not "reset" following deposition. We assume that abrasion completely removes the He-depleted rim that developed during the first stage of the grain's history. We also assume that this abrasion occurs instantaneously at the time of deposition of the grain (i.e., transport and abrasion occur over a small fraction of the grain's history). The solution requires independent knowledge of the stratigraphic age of the sedimentary unit to constrain the timing of the abrasion event. In the case of the Navajo sandstone, we use a stratigraphic age of 190 Ma (Peterson and Pipiringos, 1979). Our model assumes that parent nuclides are uniformly distributed except along the rim. A more sophisticated model is necessary for cases where zircons are complexly zoned with respect to U and Th concentrations.

Farley et al. (1996) demonstrated that the corrected He age can be determined simply by dividing the measured He age (which is the age determined using the observed U, Th, and He concentrations) by the "retentivity" (F_t). Retentivity is a function of the surface area/volume ratio of the crystal and can be calculated from the morphology of the grain. We note that the ζ-ejection correction should be applied to the He concentration rather than the measured He age. However, in practice, these two methods yield similar results except for very old (on the order of 1 Ga) He ages, where application of the F_t correction to the measured age will begin to significantly overestimate the actual age (on the order of 10%).

In the case of an abraded detrital grain, the ζ-ejection correction only needs to be applied to the post-abrasion "measured age" (i.e., the stratigraphic age). We solve for what "measured age" would need to be corrected to yield the stratigraphic age. This fraction of the observed "measured age" does not need to be corrected for alpha ejection. Let A_c represent the corrected helium age, A_d represent the depositional age of the sedimentary host, A_{pd} represent the time in a grains history between closure of the helium system and its deposition (the "pre-depositional component of the age), and A_m represent the measured age.

$A_c = A_d + A_{pd}$

We solve for A_m' (the part of the total measured age that needs to be corrected)

$A_m' = A_d \times F_t$

$A_{pd} = A_m - A_m'$

$A_c = A_d + A_m - (F_t \times A_d)$

$$\boldsymbol{A_c = A_d \times (1 - F_t) + A_m}$$

Application of the standard correction procedure to abraded grains will over-correct the ages, resulting in overestimates of actual He ages potentially by 30% or more (Fig. DR3).

To test this model, we created a Monte-Carlo simulation of ζ-ejection and grain abrasion. The model considers the crystal as a rectangular cylinder. Cartesian coordinates are randomly selected for one million parent atoms of ^{238}U, ^{235}U, and ^{232}Th. Radioactive decay is allowed to proceed for a specified period of time, t_1, representing the interval between initial closure of the He system and the time of exposure of the grain at the surface. If a given parent atom is selected to decay, the locations of 6 to 8 (depending on the type of parent) He nuclides are generated by randomly selecting a direction for displacement of the daughter and using the stopping distances reported by Farley et al. (1996).

The volume of the crystal is then reduced to simulate the effects of grain abrasion (see Fig. DR4, A-D). Abrasion first removes the corners of the grains, preserving the faces of the rectangular cylinder. The "abrasion index" corresponds to the radius of the circle used to trim the corners of the grain. After the corners are completely removed (the volume is now a regular cylinder) further abrasion is simulated by shrinking the radius of the cylinder. Decay then proceeds for a time, t_2, which represents the interval of time between deposition and the modern day. As before, final coordinates for the He nuclides are determined by randomly selecting a displacement direction and using the relevant stopping distances.

The number of parent and daughter nuclides within the final volume can be used to calculate the "measured age," which suffers from an ζ-ejection bias. Both the standard correction factor and the abrasion model can be applied and compared with the imposed age. In cases where no abrasion of the grain has occurred, the standard correction factor accurately corrects the age, whereas the abrasion correction factor underestimates the actual age. In cases where abrasion of the crystal removes part, but not all, of the original He-depleted rim, the actual age will be bracketed by ages predicted by the two different correction factors. In cases where abrasion has sufficiently removed the He-depleted rim, the abrasion correction factor accurately corrects the measured age, whereas the standard correction factor overestimates the age. Results for one set of numerical experiments are shown in Fig. DR4. Other experiments with different model parameters yielded similar results.

Thus, the numerical model confirms that the method developed here accurately corrects (U-Th)/He ages for ζ-ejection biases in cases where abrasion removes the He depleted rim. However, it is necessary to examine the morphology of the detrital grains to estimate how abrasion has altered the shape of the grain. In the case of the Navajo grains, eolian processes have clearly rounded and worn away the edges of the grains. However, in the case of fluvial

sediments, individual detrital grains may experience little abrasion. In those circumstances, the standard formula of Farley et al. (1996) should be applied. In situations where the original He-depleted rim has been partially removed, the two formulas will bracket the "true" He age.

Both the standard and detrital alpha ejection corrections assume that the parent atoms are homogeneously distributed throughout the sample. However, U-Th zonation is commonly observed in zircons, and may introduce significant errors into the ζ-ejection correction (e.g., Tagami et al., 2003). To assess the styles and extents of zonation in the Navajo Sandstone zircons, we obtained back-scattered electron (BSE) and cathodoluminescence (CL) images for a suite of randomly selected grains (Fig. DR5). In general, regions of zircon with high BSE and low CL intensities have relatively high U contents, although the magnitude of U-concentration contrast does not simply scale with brightness contrast in BSE or CL. In these samples, we observed a wide variety of zonation styles and apparent extents, but in most cases the zonation was not concentric with respect to the external morphology of the grain. These observations indicate that ζ-ejection biases due to U-zonation will generally be negligible.

REFERENCES CITED

Black, L.P., Kamo, S.L, Allen, C.M., Davis, D.W., Aleinikoff, J.N., Valley, J.W., Mundil, R., Campbell, I.H., Korsch, R.J., Williams, I.S., and Foudoulis, C., Towards more reliable Pb/U micro-probe geochronology: SHRIMP, ID-TIMS, ELA-ICP-MS, and oxygen isotope documentation for a series of zircon standards: Chemical Geology (in review).

Cumming G.L. and Richards, J.R., 1975, Ore lead isotope ratios in a continuously changing earth: Earth and Planetary Science Letters, v. 28, p. 155-171.

Eggins, S.M. and Shelley, J.M.G., 2002, Compositional heterogeneity in NIST SRM 610-617 glasses: Geostandards Newsletter, v. 26, p. 269-286.

Farley, K.A., Wolf, R.A., and Silver, L.T., 1996, The effects of long alpha-stopping distances on (U-Th)/He ages: Geochimica et Cosmochimica Acta, v. 60, p. 4223-4229.

Peterson, F., and Pipiringos, G.N., 1979, Stratigraphic relations of the Navajo Sandstone to Middle Jurassic formations, southern Utah and northern Arizona: U.S. Geological Survey Professional Paper 1035-B, p. B1–B43.

Tagami, T., Farley, K.A., and Stockli, D.F., 2003, (U-Th)/He geochronology of single zircon grains of known Tertiary eruption age: Earth and Planetary Science Letters, v. 6531, p. 1-11.

ACKNOLWEDGEMENTS

We thank Mike Breeding and Jeremey Hourigan for guidance in preparing the CL grain mount and Jim Eckert for his assistance in obtaining the CL images.

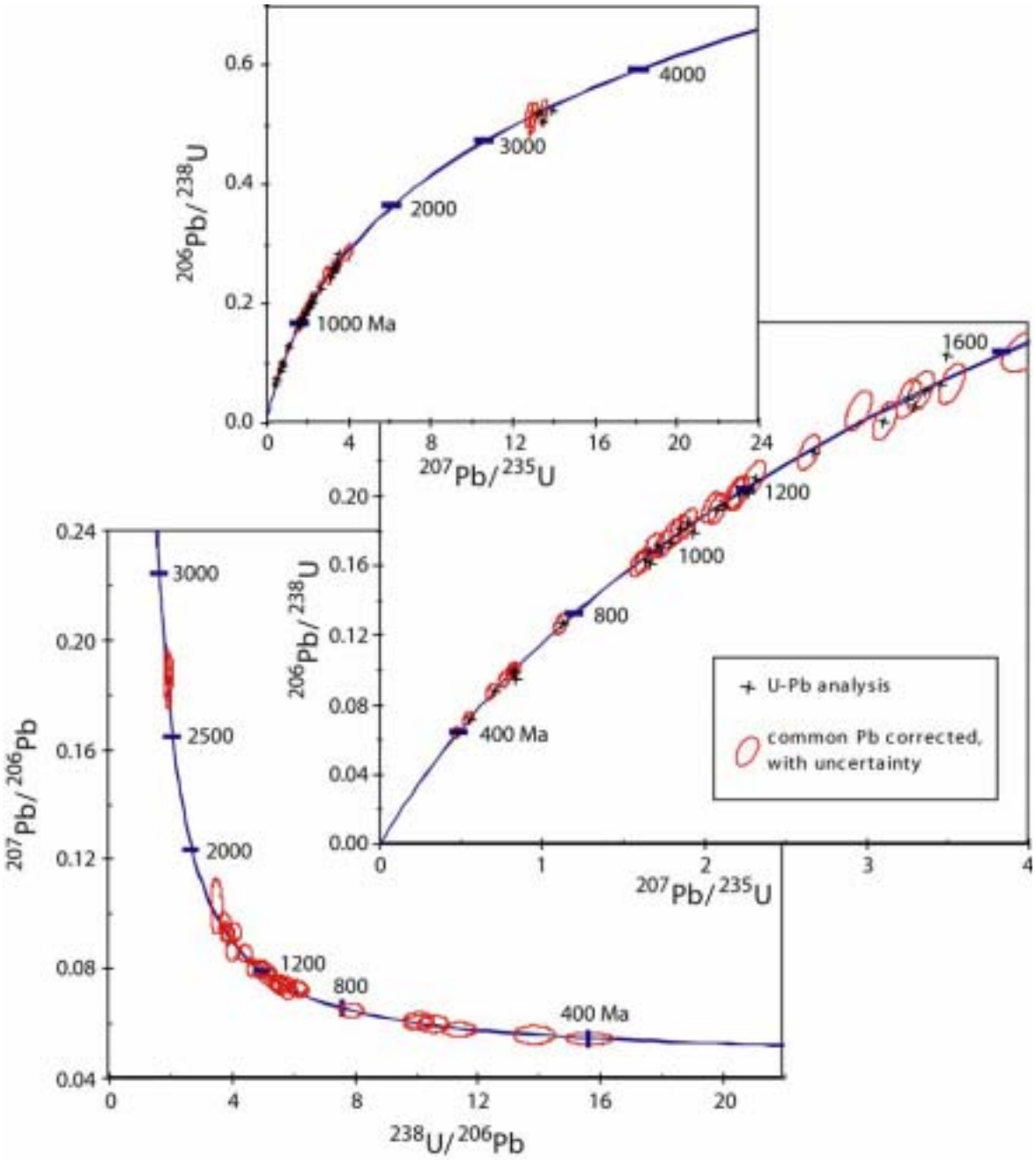

Figure DR1. U/Pb plots for Navajo grains in this study, with ellipses representing 1 ω uncertainty.

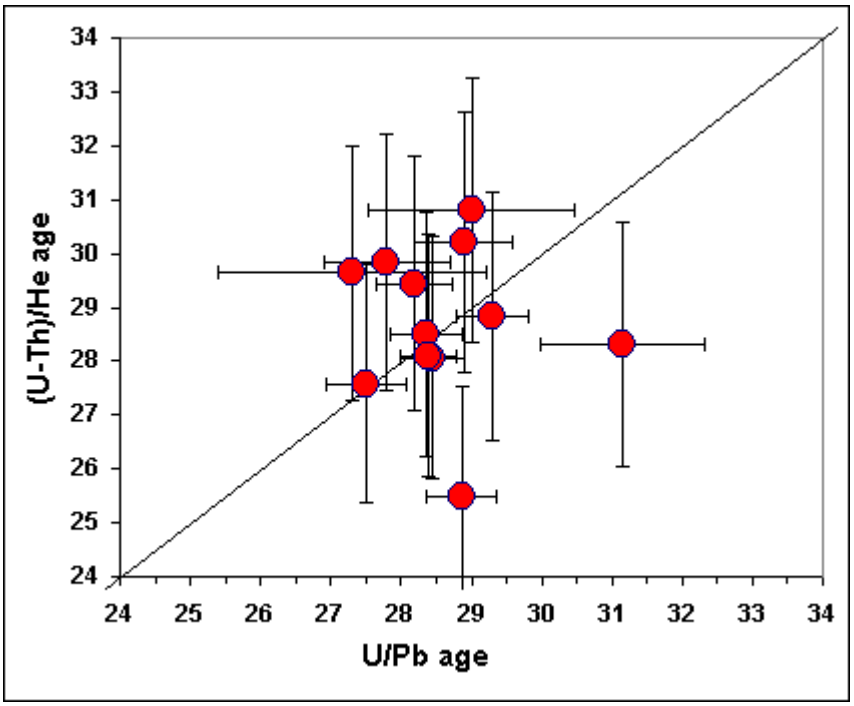

Figure DR2. Combined He-Pb plot for single zircons from the Fish Canyon Tuff. Bulk crystal (U-Th)/He ages are unaffected by the laser-ablation process.

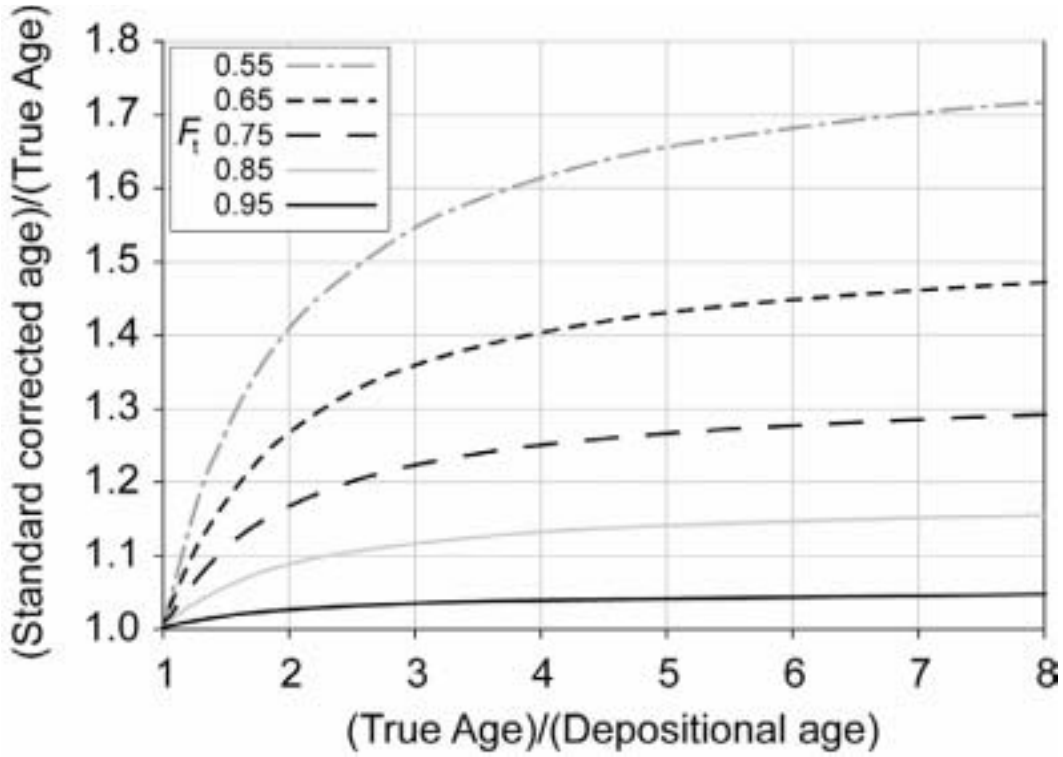

Figure DR3. Error caused by the use of the standard ζ-ejection correction to grains for which the detrital ζ-ejection correction formula described in this appendix is applicable. The *y*-axis shows the overestimate of the standard correction relative to the true age of the grain. The *x*-axis shows the true age of the sample, normalized against the depositional age. Thus, the greater the true age of the sample, the larger the absolute error. For example, for a grain with a F_t of 0.65 and a True Age equal to 4 times its Depositional Age, the standard correction factor will overestimate the True Age by 40%.

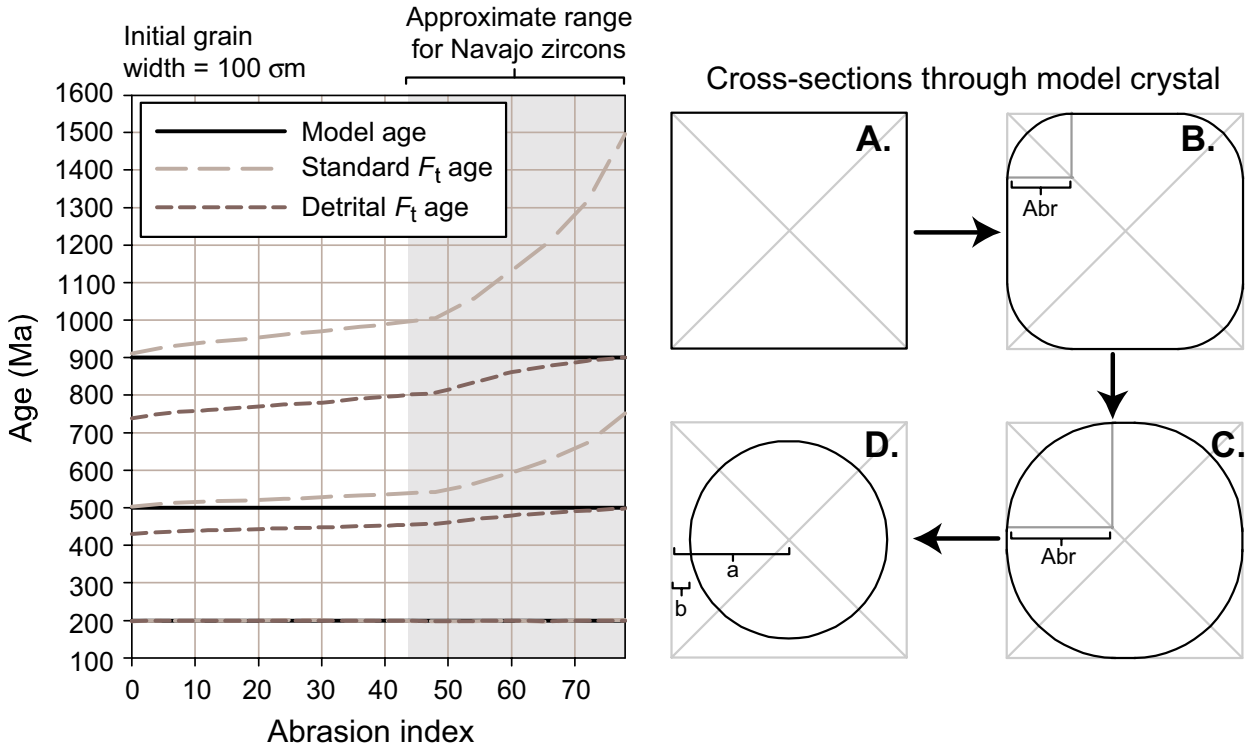

Figure DR4. Results from three Monte-Carlo simulations of ζ-ejection. The initial grain width is set to 100 σm, and the time of deposition, t_2, is set to 200 Ma. The time prior to deposition, t_1, was set to 0 myr, 300 myr, and 700 myr. For each model, the ages obtained by use of the standard and detrital ζ-ejection corrections are shown as a function of the "abrasion index." In the initial phases of rounding, the abrasion index corresponds to the radius of a circle used to trim the corner of the grain ("Abr" in B and C). When the corners are completely removed, further abrasion is simulated by reducing the radius of the cross-sectional circle (D). In D, the "abrasion index" is the sum of segments "a" and "b." The range for the Navajo zircons, based on visual examination of grain morphology, is shown in grey. If no time elapses prior to deposition (e.g., volcanic grains, or cases where the He-clock is "reset" post-deposition due to heating above the closure temperature), then both ζ-ejection corrections yield the same ages. However, when t_1 is greater than zero, the simulations show that the age calculated using the standard approach will slightly overestimate the actual age of the grain and the detrital ζ-ejection will yield an underestimate. If grain abrasion is significant (as in the case of the Navajo grains), the standard approach leads to a significant overestimate of the true age, while the detrital ζ-ejection approach converges on the actual age.

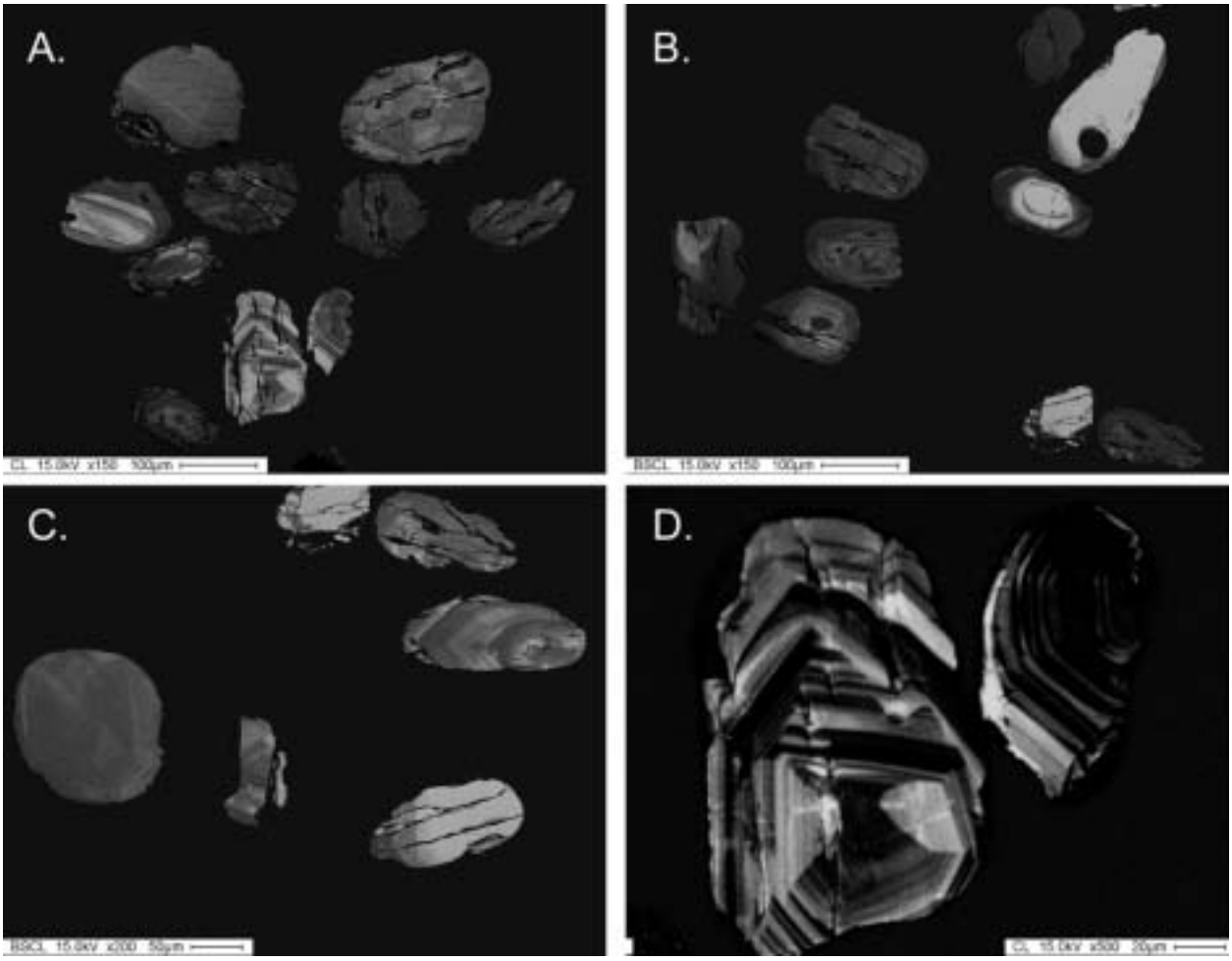

Figure DR5. A-C: Combined BSE and CL images of zircons from the Navajo Sandstone. D: CL only image of two highly zoned zircons.

Sample	Pb*(ppm)	Th/U	U (ppm)	uncorr'd 206Pb/238U ratio	± 1ω	208Pb corr'd 206Pb*/238U ratio	%common 206Pb using 208Pb
NAV1-01	61.6	1.350	91	0.50345	0.00268	0.50130	0.42703
NAV1-02	11.3	0.351	123	0.09028	0.00046	0.08996	0.35078
NAV1-03	25.3	0.109	419	0.06387	0.00031	0.06379	0.13774
NAV1-04	109.3	0.351	190	0.51633	0.00283	0.51483	0.29193
NAV1-05	92.5	0.704	150	0.51620	0.00289	0.51533	0.16861
NAV1-06	110.7	0.345	562	0.19221	0.00074	0.19223	-0.00953
NAV1-07	16.2	0.474	76	0.20107	0.00112	0.20085	0.11050
NAV1-08	33.6	0.536	138	0.22502	0.00107	0.22477	0.10947
NAV1-09	33.3	1.995	48	0.46691	0.00260	0.46320	0.80035
NAV1-10	94.0	0.354	498	0.18376	0.00085	0.18379	-0.01464
NAV1-11	72.7	0.183	457	0.16278	0.00062	0.16272	0.03690
NAV1-12	12.5	0.979	103	0.10176	0.00073	0.10147	0.28119
NAV1-13	20.8	0.805	101	0.18011	0.00108	0.18012	-0.00519
NAV1-14	25.6	0.475	193	0.12626	0.00064	0.12619	0.05717
NAV1-15	11.4	0.813	58	0.17038	0.00104	0.17011	0.16432
NAV1-16	16.1	0.547	172	0.08755	0.00042	0.08736	0.21383
NAV1-17	103.9	0.578	359	0.26363	0.00119	0.26418	-0.20610
NAV1-18	96.1	0.358	1392	0.06559	0.00263	0.05972	9.82583
NAV1-19	115.7	0.359	555	0.20187	0.00373	0.20137	0.24946
NAV1-20	37.0	1.062	116	0.25992	0.00120	0.25974	0.07270
NAV2-01	5.8	0.595	29	0.17878	0.00160	0.17779	0.55984
NAV2-02	16.2	0.337	98	0.16141	0.00104	0.16084	0.35404
NAV2-03	25.1	0.845	220	0.09880	0.00061	0.09871	0.09063
NAV2-04	17.8	0.544	89	0.18582	0.00104	0.18567	0.08312
NAV2-05	57.1	2.309	69	0.51944	0.00175	0.51826	0.22811
NAV2-06	102.9	0.118	412	0.25568	0.00098	0.25570	-0.00739
NAV2-07	8.3	0.878	116	0.06122	0.00049	0.06096	0.42407
NAV2-08	20.5	1.403	218	0.07197	0.00044	0.07193	0.06568
NAV2-09	28.6	0.537	154	0.17269	0.00086	0.17237	0.18960
NAV2-10	121.2	1.531	428	0.21008	0.00094	0.21003	0.02468
NAV2-11	18.6	0.489	72	0.24241	0.00128	0.24251	-0.04070
NAV2-12	21.9	0.620	99	0.20138	0.00112	0.20101	0.18367
NAV2-13	5.2	0.677	18	0.25115	0.00253	0.24857	1.03765
NAV2-14	35.3	0.369	176	0.19367	0.00087	0.19305	0.32103
NAV2-15	68.5	0.716	215	0.28144	0.00137	0.28352	-0.73359
NAV2-16	8.5	0.484	85	0.09496	0.00071	0.09440	0.59080
NAV2-17	27.0	1.559	71	0.28019	0.00172	0.28403	-1.35388
NAV2-18	41.6	0.754	130	0.27949	0.00207	0.27987	-0.13507
NAV2-19	23.9	0.694	218	0.09878	0.00061	0.09875	0.03007
NAV2-20	17.7	0.722	153	0.10342	0.00065	0.10366	-0.23666

Table DR1. U/Pb data (1 of 3)

uncorr'd 207Pb/235U ratio	± 1ω	208Pb corr'd 207Pb*/235U ratio	uncorr'd 207Pb/206Pb ratio	± 1ω	208Pb corr'd 207Pb*/206Pb* ratio	uncorr'd 208Pb/232Th	± 1ω
13.29752	0.12098	12.97714	0.19157	0.00141	0.18775	0.14137	0.00089
0.78651	0.01902	0.74745	0.06319	0.00149	0.06026	0.02966	0.00045
0.48705	0.00634	0.47637	0.05530	0.00067	0.05416	0.02161	0.00039
13.07496	0.11592	12.85126	0.18366	0.00128	0.18104	0.15216	0.00286
13.19392	0.10964	13.06429	0.18538	0.00114	0.18387	0.14465	0.00124
2.08111	0.01497	2.08348	0.07852	0.00048	0.07861	0.05748	0.00034
2.22539	0.03666	2.19659	0.08027	0.00124	0.07932	0.06111	0.00083
2.68136	0.02514	2.64902	0.08642	0.00070	0.08547	0.06774	0.00058
12.02789	0.12391	11.47674	0.18683	0.00162	0.17970	0.13203	0.00094
1.89735	0.01561	1.90081	0.07488	0.00051	0.07501	0.05522	0.00049
1.64073	0.01396	1.63305	0.07310	0.00056	0.07279	0.04992	0.00048
0.91507	0.01893	0.87950	0.06522	0.00127	0.06286	0.03176	0.00035
1.84816	0.03165	1.84936	0.07442	0.00119	0.07447	0.05425	0.00047
1.13235	0.01557	1.12331	0.06504	0.00083	0.06456	0.03894	0.00036
1.72304	0.03826	1.68738	0.07334	0.00157	0.07194	0.05214	0.00058
0.71626	0.01185	0.69332	0.05934	0.00094	0.05756	0.02781	0.00032
3.45564	0.02385	3.52874	0.09507	0.00050	0.09688	0.07530	0.00058
1.10199	0.07435	0.40154	0.12186	0.00661	0.04877	0.04934	0.00121
2.28014	0.04679	2.21490	0.08192	0.00073	0.07977	0.06325	0.00067
3.36261	0.04314	3.33742	0.09383	0.00112	0.09319	0.07677	0.00061
1.93634	0.04807	1.80879	0.07855	0.00182	0.07379	0.05720	0.00119
1.67431	0.03004	1.60161	0.07523	0.00126	0.07222	0.05233	0.00087
0.82697	0.01358	0.81590	0.06070	0.00092	0.05995	0.03069	0.00025
2.07843	0.02816	2.05836	0.08112	0.00100	0.08040	0.05614	0.00058
13.73978	0.09615	13.56256	0.19184	0.00118	0.18980	0.14333	0.00099
3.25841	0.02231	3.26093	0.09243	0.00053	0.09249	0.07566	0.00108
0.47113	0.01200	0.43989	0.05581	0.00135	0.05233	0.01973	0.00024
0.55689	0.00866	0.55112	0.05612	0.00080	0.05557	0.02246	0.00019
1.79912	0.02514	1.75723	0.07556	0.00099	0.07394	0.05328	0.00055
2.32038	0.01711	2.31365	0.08011	0.00047	0.07989	0.06287	0.00044
3.10261	0.03735	3.11577	0.09283	0.00100	0.09318	0.07092	0.00079
2.26313	0.03044	2.21517	0.08151	0.00100	0.07993	0.06141	0.00073
3.29477	0.08074	2.95529	0.09515	0.00213	0.08623	0.08174	0.00131
2.13026	0.02340	2.05026	0.07978	0.00080	0.07703	0.06190	0.00098
3.85075	0.04112	4.13421	0.09924	0.00094	0.10576	0.07581	0.00077
0.84375	0.02177	0.77486	0.06444	0.00159	0.05953	0.03159	0.00067
3.49614	0.04332	4.01753	0.09050	0.00097	0.10259	0.07764	0.00057
3.98745	0.08222	4.03888	0.10347	0.00199	0.10467	0.08018	0.00081
0.83549	0.01604	0.83181	0.06134	0.00112	0.06109	0.03051	0.00027
0.81008	0.01508	0.84031	0.05681	0.00100	0.05879	0.03135	0.00033

Table DR1. U/Pb data (2 of 3)

208Pb corr'd 207Pb*/206Pb* age (Ma)	± 1ω	208Pb corr'd 206Pb*/238U age (Ma)	± 1ω	Comment
2722.5	70.9	2623.2	101.4	
612.7	20.4	555.6	21.5	Discordant
378.1	10.7	398.7	15.4	
2662.5	68.9	2677.9	103.5	
2688.1	69.5	2681.2	103.7	
1162.2	30.3	1133.9	43.7	
1180.2	33.4	1180.6	45.7	
1326.3	35.1	1307.9	50.5	
2650.1	71.0	2459.5	95.4	Discordant
1068.8	29.4	1088.1	42.1	
1008.0	26.5	972.1	37.5	
703.5	26.2	623.8	24.4	Discordant
1054.2	34.2	1068.7	41.5	
760.2	21.6	766.6	29.7	
984.4	31.7	1013.8	39.4	
513.2	16.4	540.3	20.9	
1564.8	41.0	1512.2	58.4	
137.4	27.7	374.6	20.7	Discordant
1191.5	32.3	1182.7	49.6	
1491.8	43.0	1490.4	57.6	
1035.7	35.0	1055.7	41.5	
992.3	28.5	961.9	37.4	
601.7	19.0	607.5	23.6	
1206.9	33.0	1098.6	42.6	Discordant
2740.4	72.4	2698.8	104.1	
1477.5	38.7	1468.0	56.6	
300.3	13.3	381.9	15.0	Discordant
435.5	19.6	448.6	17.5	
1039.8	29.1	1025.8	39.7	
1194.4	35.3	1231.3	47.6	
1491.6	39.8	1400.5	54.2	
1195.2	33.2	1181.6	45.8	
1343.3	43.5	1432.5	56.6	
1121.9	30.4	1138.4	44.0	
1727.5	46.3	1610.7	62.3	Discordant
586.6	22.4	581.9	22.8	
1671.4	129.7	1614.0	67.3	
1708.4	47.7	1591.3	62.0	Discordant
642.4	20.2	607.6	23.6	
559.5	18.1	636.4	24.7	Discordant

Table DR1.U/Pb data (2 of 3)

Sample	U (ng)	Th (ng)	Th/U	He (nmol)	Radius (σm)	Ft	Measured age (Ma)	Corrected age (Ma)	2ω error (Ma)
0203151A	1.73	0.606	0.35	292	38	0.753	178	223	18
0203151B	0.362	0.308	0.85	171	40	0.744	355	401	32
0203151C	4.01	1.31	0.33	537	46	0.786	207	246	20
0203151D	1.32	0.531	0.40	208	54	0.804	273	309	25
0203152A	0.147	0.109	0.75	116	35	0.713	400	452	36
0203152B	0.349	0.432	1.2	141	42	0.749	294	339	27
0203152C	0.743	0.397	0.53	304	37	0.732	283	331	27
NAV1-1	0.996	0.896	0.90	389	80	0.852	1286	1314	105
NAV1-4	1.90	0.404	0.21	510	77	0.854	1066	1093	87
NAV1-5	0.889	0.794	0.89	968	48	0.785	1296	1337	107
NAV1-6	2.07	0.419	0.20	311	63	0.819	319	354	28
NAV1-7	0.592	0.232	0.39	231	40	0.752	342	390	31
NAV1-8	0.776	0.244	0.31	213	54	0.805	473	511	41
NAV1-10	1.33	0.470	0.35	241	49	0.781	214	256	20
NAV1-20	0.675	0.530	0.79	512	48	0.777	799	842	67
NAV2-1	0.278	0.160	0.57	40.5	55	0.808	265	301	24
NAV2-2	0.583	0.154	0.26	120	60	0.811	374	410	33
NAV2-3	0.326	0.237	0.73	130	43	0.754	319	366	29
NAV2-5	0.365	0.722	2.0	340	51	0.790	1047	1087	87
NAV2-6	1.80	0.432	0.24	442	52	0.793	353	392	31
NAV2-8	0.855	1.09	1.3	142	51	0.784	184	225	18
NAV2-9	0.863	0.324	0.38	166	51	0.787	307	348	28
NAV2-16	0.618	0.285	0.46	92.2	53	0.806	284	320	26
NAV2-19	1.60	0.276	0.17	290	62	0.827	463	496	40

Table DR2. (U-TH)/He data